

## Silicon-Vacancy Spin Qubit in Diamond: A Quantum Memory Exceeding 10 ms with Single-Shot State Readout

D. D. Sukachev,<sup>1,\*</sup> A. Sipahigil,<sup>1</sup> C. T. Nguyen,<sup>1</sup> M. K. Bhaskar,<sup>1</sup> R. E. Evans,<sup>1</sup> F. Jelezko,<sup>2</sup> and M. D. Lukin<sup>1,†</sup>

<sup>1</sup>*Department of Physics, Harvard University, 17 Oxford Street, Cambridge, Massachusetts 02138, USA*

<sup>2</sup>*Institute for Quantum Optics, Ulm University and Center for Integrated Quantum Science and Technology, Albert-Einstein-Allee 11, 89081 Ulm, Germany*

(Received 29 August 2017; published 29 November 2017)

The negatively charged silicon-vacancy ( $\text{SiV}^-$ ) color center in diamond has recently emerged as a promising system for quantum photonics. Its symmetry-protected optical transitions enable the creation of indistinguishable emitter arrays and deterministic coupling to nanophotonic devices. Despite this, the longest coherence time associated with its electronic spin achieved to date ( $\sim 250$  ns) has been limited by coupling to acoustic phonons. We demonstrate coherent control and suppression of phonon-induced dephasing of the  $\text{SiV}^-$  electronic spin coherence by 5 orders of magnitude by operating at temperatures below 500 mK. By aligning the magnetic field along the  $\text{SiV}^-$  symmetry axis, we demonstrate spin-conserving optical transitions and single-shot readout of the  $\text{SiV}^-$  spin with 89% fidelity. Coherent control of the  $\text{SiV}^-$  spin with microwave fields is used to demonstrate a spin coherence time  $T_2$  of 13 ms and a spin relaxation time  $T_1$  exceeding 1 s at 100 mK. These results establish the  $\text{SiV}^-$  as a promising solid-state candidate for the realization of quantum networks.

DOI: 10.1103/PhysRevLett.119.223602

Quantum networks require the ability to store quantum information in long-lived memories, to efficiently interface these memories with optical photons, and to provide quantum nonlinearities required for deterministic quantum gate operations [1,2]. Even though key building blocks of quantum networks have been demonstrated in various systems [3,4], no solid-state platform has satisfied these requirements. Over the past decade, solid-state quantum emitters with stable spin degrees of freedom such as charged quantum dots and nitrogen-vacancy (NV) centers in diamond have been investigated for the realization of quantum network nodes [5]. While quantum dots can be deterministically interfaced with optical photons [6], their quantum memory time is limited to the microsecond scale [7] due to interactions with their surrounding nuclear spin bath. In contrast, NV centers have an exceptionally long-lived quantum memory [8] but suffer from weak, spectrally unstable optical transitions [9]. Despite impressive proof-of-concept experimental demonstrations with these systems [10,11], scaling to a large number of nodes is limited by the challenge of identifying suitable quantum emitters with the combination of strong, homogeneous, and coherent optical transitions and long-lived quantum memories.

The negatively charged silicon-vacancy ( $\text{SiV}^-$ ) centers in diamond has recently been shown to have bright, narrow-band optical transitions with a small inhomogeneous broadening [12,13]. The optical coherence of the  $\text{SiV}^-$  is protected by its inversion symmetry [14], even in nanostructures [15]. These optical properties were recently used to show strong interactions between single photons and single  $\text{SiV}^-$  centers and to probabilistically entangle two  $\text{SiV}^-$  centers in a single

nanophotonic device [16]. At 4 K, however, the  $\text{SiV}^-$  spin coherence is limited to  $\sim 100$  ns due to coupling to the phonon bath, mediated by the spin-orbit interaction [17–21].

In this Letter, we demonstrate high-fidelity coherent manipulation and single-shot readout of individual  $\text{SiV}^-$  spin qubits in a dilution refrigerator. In particular, we extend the coherence time of the  $\text{SiV}^-$  electronic spin by 5 orders of magnitude to 13 ms by operating at 100 mK [22].

The key idea of the present work can be understood by considering the energy-level diagram of the  $\text{SiV}^-$  [Fig. 1(a)]. The ground state of the  $\text{SiV}^-$  is split by the spin-orbit interaction and crystal strain into a lower branch (LB) and an upper branch (UB) separated by  $\Delta_{\text{GS}}$ . Each branch comprises two degenerate spin sublevels [24]. Application of a magnetic field lifts the spin degeneracy and allows the use of the spin sublevels  $|\downarrow\rangle$  and  $|\uparrow\rangle$  of the LB as qubit states. At 4 K, the  $\text{SiV}^-$  spin coherence is limited to  $\sim 100$  ns [17–21] due to interactions with the thermal acoustic phonon bath at frequency  $\Delta_{\text{GS}} \sim 50$  GHz. These interactions result in a relaxation at rates  $\gamma_+$  and  $\gamma_-$  between the levels in the LB and the UB with different orbitals and the same spin projections as shown in Fig. 1(a), which destroys spin coherence. By reducing the occupation of phonon modes at  $\Delta_{\text{GS}}$  at lower temperatures, one can suppress the rate  $\gamma_+$ , leaving the spin qubit in a manifold free from phonon-induced decoherence, thereby increasing spin coherence [19].

We investigate the  $\text{SiV}^-$  properties below 500 mK using a dilution refrigerator with a free-space confocal microscope and a vector magnet as shown in Fig. 1(b). Details of the experimental setup are available in the Supplemental Material [25]. We first study the thermal population of the

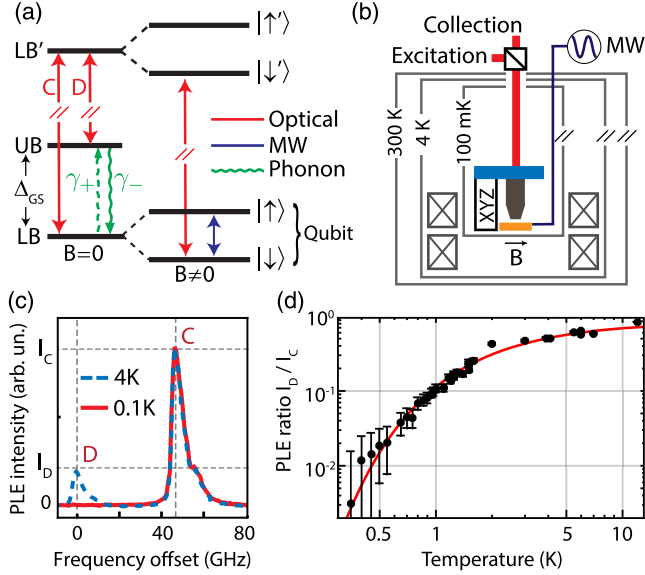


FIG. 1. (a)  $\text{SiV}^-$  electronic structure. Optical transitions  $C$  and  $D$  connect the lower (LB) and upper (UB) spin-orbit branches to the lowest energy optical excited state (LB'). Each branch is split into two spin sublevels in a magnetic field  $\vec{B}$ . Red and blue arrows denote optical and microwave transitions, respectively.  $\gamma_+$  and  $\gamma_-$  are phonon-induced decay rates. (b) Schematic of the setup. An objective is mounted on piezo positioners to image the diamond sample using free-space optics. The combined system is attached to the mixing plate of a dilution refrigerator and placed inside a superconducting vector magnet. (c) PLE spectra of an  $\text{SiV}^-$  ensemble at  $B = 0$  for  $T = 4$  K and 0.1 K. The peak intensity  $I_C$  ( $I_D$ ) is proportional to the population in the LB (UB). (d)  $I_D/I_C$  (and  $\gamma_+/\gamma_-$ ) is reduced at low temperatures, following  $e^{-h\Delta/k_B T}$  with  $\Delta_{\text{fit}} = 42 \pm 2$  GHz in agreement with the measured  $\Delta_{\text{GS}} = 48$  GHz.

LB and the UB between 0.1 and 10 K using an ensemble of as-grown  $\text{SiV}^-$  centers (sample A in Ref. [23]). We probe the relative populations in the LB and the UB by measuring the ensemble photoluminescence excitation (PLE) spectra of transitions  $C$  and  $D$ . Transitions  $C$  and  $D$  are both visible in PLE at 4 K, which suggests comparable thermal population in the LB and UB [Fig. 1(c)]. As the temperature is lowered [Fig. 1(d)], the ratio of the transition  $D$  and  $C$  peak amplitudes ( $I_D/I_C$ ) reduces by more than 2 orders of magnitude and follows  $e^{-h\Delta_{\text{GS}}/k_B T}$  [19]. These measurements demonstrate an orbital polarization in the LB of  $>99\%$  below 500 mK. At these low temperatures,  $\gamma_+ \ll \gamma_-$ , and the qubit states are effectively decoupled from the phonon bath.

To investigate the coherence properties of single emitters, we create single  $\text{SiV}^-$  centers at a depth of  $\sim 250$  nm via  $^{28}\text{Si}$  ion implantation at a dose of  $10^9 \text{ cm}^{-2}$  and an energy of 380 keV into two type-IIa ( $[\text{N}] < 5$  ppb,  $[\text{B}] < 1$  ppb) diamond samples (Element Six). The first sample (sample 13) has a natural abundance of 1.1% of  $^{13}\text{C}$  isotopes with a nuclear spin  $I = 1/2$ . The second sample

(sample 12) is engineered to have only  $10^{-3}\%$   $^{13}\text{C}$  to suppress hyperfine interactions between the spin qubit and the nuclear spin bath [8]. After ion implantation and high-temperature annealing [15], we fabricate a shorted coplanar waveguide on the diamond to drive microwave (MW) transitions between the qubit states [25].

We use spin-selective optical transitions between states  $|i\rangle$  and  $|i'\rangle$  at frequencies  $f_{ii'}$  ( $i = \{\uparrow, \downarrow\}$ ) [Fig. 2(a)] to optically initialize and read out the qubit states. Applying a magnetic field  $B \sim 0.5\text{--}3$  kG allows us to optically resolve these transitions. Figure 2(b) shows the PLE spectrum of the spin-selective optical transitions at 4 K (red circles). These resonances disappear in continuous wave measurements at 100 mK (blue squares). This effect results from optical pumping of the qubit to the long-lived dark spin state. The central peak originates from off-resonant scattering from the two spin transitions.

To achieve high-fidelity readout of the spin states, it is desirable to scatter photons many times without causing a spin flip [28,29]. To obtain such spin-conserving optical transitions, the cyclicity of the transition  $\gamma_{\parallel}/(\gamma_{\perp} + \gamma_{\parallel})$

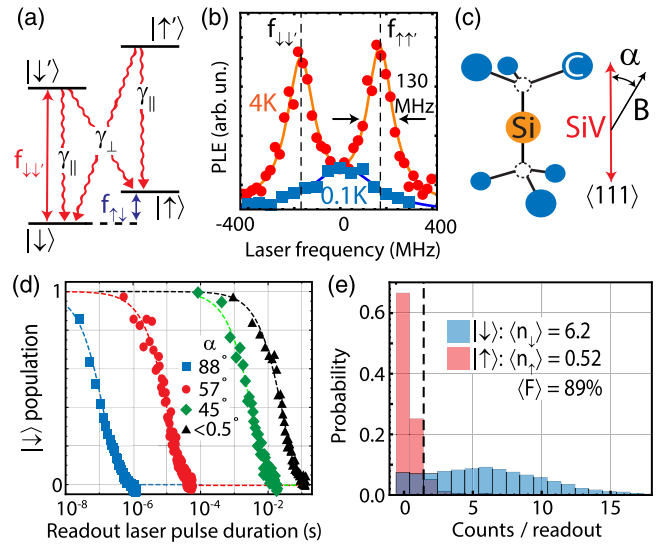


FIG. 2. (a) Spin-selective optical transitions and branching ratios.  $f_{ij}$  is the transition frequency between states  $i$  and  $j$ .  $\gamma_{\parallel}$  and  $\gamma_{\perp}$  are spin-conserving and spin-flipping decay rates, respectively;  $f_{\uparrow\downarrow}$  is the qubit frequency. (b) PLE spectra measured at 4 and 0.1 K. (c) Schematic of the  $\text{SiV}^-$  molecular structure [24].  $\alpha$  is the angle between the magnetic field  $\vec{B}$  and the  $\text{SiV}^-$  symmetry axis set by the two lattice vacancies (empty circles) and aligned along the  $\langle 111 \rangle$  diamond axis. (d) Optical spin pumping time scale  $\tau$  measured at different  $\vec{B}$ . Here,  $\{\alpha, B, \tau\} = \{88^\circ, 2.9 \text{ kG}, 140 \text{ ns}\}$  for the blue squares;  $\{57^\circ, 3.0 \text{ kG}, 10 \mu\text{s}\}$  for the red circles;  $\{45^\circ, 1.7 \text{ kG}, 3 \text{ ms}\}$  for the green diamonds; and  $\{<0.5^\circ, 2.7 \text{ kG}, 30 \text{ ms}\}$  for the black triangles. (e) Single-shot spin readout in  $B = 2.7$  kG. A 20-ms-long laser pulse at frequency  $f_{\downarrow\downarrow'}$  is used for state readout. A second laser initializes the spin states via optical pumping. Spin readout photon statistics after initialization in state  $|\uparrow\rangle$  (red) and  $|\downarrow\rangle$  (blue). Average fidelity  $F = 89\%$ .

be tuned by varying the angle  $\alpha$  of the applied magnetic field with the SiV symmetry axis as shown in Fig. 2(c) [17]. Figure 2(d) shows the optical spin pumping time scale for different  $\alpha$  when the transition  $f_{\downarrow\downarrow}$  is driven near saturation. We extend the optical pumping time scale by more than 5 orders of magnitude, from 100 ns for  $\alpha \sim 90^\circ$  to 30 ms in an aligned field.

The ability to optically excite the SiV<sup>-</sup>  $\sim 10^5$  times without causing a spin flip [25] enables high-fidelity single-shot readout of the spin state despite the low photon collection efficiency ( $\sim 10^{-4}$ ) in the phonon sideband (PSB). We measure the spin state by driving the  $f_{\downarrow\downarrow}$  transition near saturation and monitoring fluorescence on the PSB. Figure 2(e) shows the readout count distributions for the spin initialized in the states  $|\downarrow\rangle$  (blue histogram) and  $|\uparrow\rangle$  (red histogram) using a 150-ms-long pulse from a second laser at frequency  $f_{\uparrow\uparrow}$  or  $f_{\downarrow\downarrow}$ , respectively. We detect  $\langle n_{\downarrow} \rangle = 6.2$  photons from state  $|\downarrow\rangle$  and  $\langle n_{\uparrow} \rangle = 0.52$  from state  $|\uparrow\rangle$  in a 20-ms-long readout window. By choosing a state-detection threshold of  $n > 1$  for state  $|\downarrow\rangle$  and  $n \leq 1$  for state  $|\uparrow\rangle$ , we obtain an average readout fidelity of  $F = (F_{\uparrow} + F_{\downarrow})/2 = 0.89$ , where  $F_i$  is the readout fidelity for state  $i$ . For the measurements in Figs. 3 and 4, we roughly align the magnetic field with  $\alpha < 5^\circ$  to operate in an efficient spin readout regime but do not optimize for the highest fidelity at each point. Under

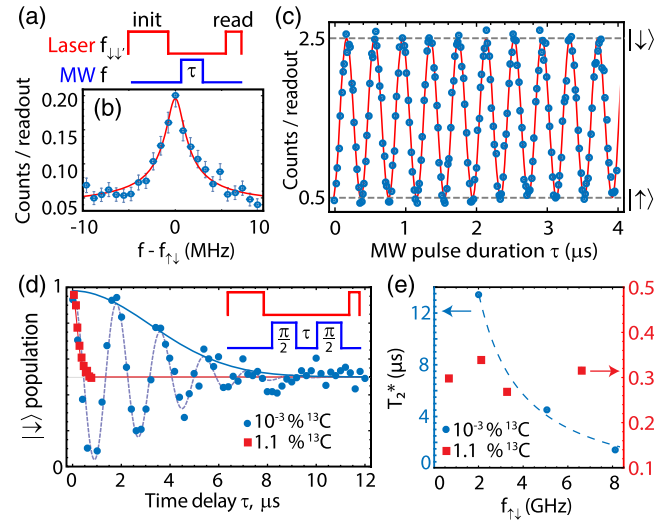


FIG. 3. (a) Pulse sequence for ODMR and Rabi measurements. (b) Pulsed ODMR measurement for  $\tau = 500 \mu\text{s}$ . Durations of the initialization and readout laser pulses are 15 and 2 ms, respectively [25]. (c) Resonant driving at frequency  $f_{\downarrow\downarrow}$  results in Rabi oscillations between the states  $|\uparrow\rangle$  and  $|\downarrow\rangle$ . Data in (b) and (c) are from sample 12. (d) Ramsey interference measurement of  $T_2^*$  for the two samples. MW pulses are detuned by  $\sim 550$  kHz from the  $f_{\downarrow\downarrow}$  transition for the blue data. Duration of the initialization (readout) laser pulse is 15 ms (2 ms) for sample 12 and 1.5 ms (0.2 ms) for sample 13. (e)  $T_2^*$  as a function of qubit resonant frequency. Dashed blue line is a fit to  $1/f_{\downarrow\uparrow}$  scaling [25].

these conditions, we measure lifetimes ( $T_1$ ) of the qubit states exceeding 1 s at 100 mK [25].

The spin readout time ( $\sim 10$  ms) is currently limited by the low collection efficiency of the setup [25] and by optical pumping to the metastable UB of the ground state [25] with a lifetime of  $\sim 200$  ns [19]. This readout time can be reduced by several orders of magnitude by adding a repumping laser on transition  $D$  [Fig. 1(a)] and by using nanophotonic structures to improve the collection efficiency to above 10% [16].

To coherently control the SiV<sup>-</sup> electron spin qubit, we use a MW field at frequency  $f_{\uparrow\downarrow}$  [21]. For the measurements shown in Figs. 2, 3, and 4, single strained SiV<sup>-</sup> centers with  $\Delta_{\text{GS}} \sim 80$  GHz are used. When crystal strain is

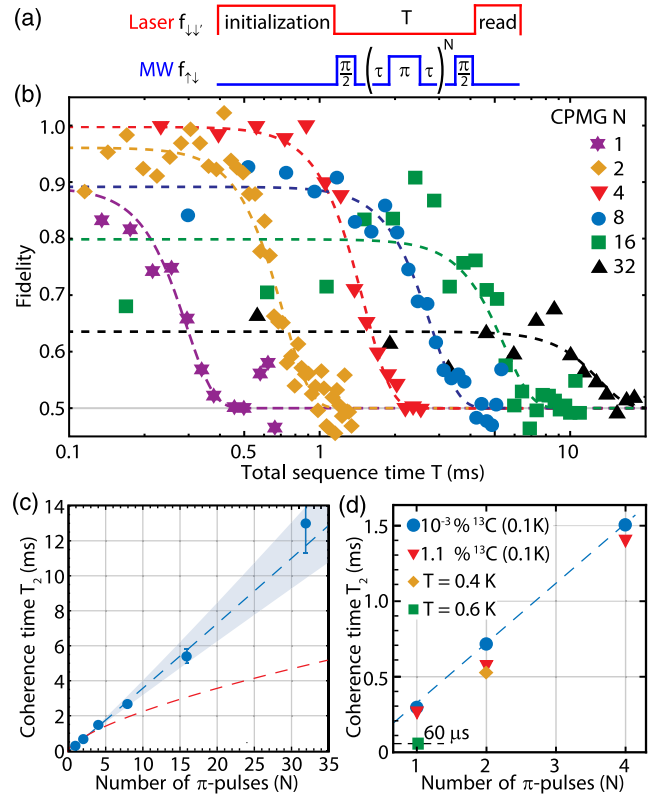


FIG. 4. 13 ms spin coherence with dynamical decoupling. (a) CPMG sequence with  $N$  rephasing MW  $\pi$  pulses. (b) Spin coherence for CPMG sequences with  $N = 1, 2, 4, 8, 16,$  and  $32$  pulses in sample 12 in an aligned magnetic field  $B \approx 1.6$  kG at 100 mK. The longest measured  $T_2$  time is 13 ms for  $N = 32$ . State fidelity reduces with higher  $N$  due to  $\pi$ -pulse errors. Durations of the initialization and readout laser pulses are  $\sim 100$  ms and  $\sim 15$  ms, correspondingly. Dashed lines are fits to  $\exp[-(T/T_2)^4]$  [25]. (c)  $T_2$  coherence vs number of rephasing pulses  $N$  for sample 12. Fitting to  $T_2 \propto N^\beta$  gives  $\beta = 1.02 \pm 0.05$  (blue dashed line); the shaded region represents a standard deviation of 0.05. For comparison, the red dashed line shows  $N^{2/3}$  scaling. (d)  $T_2$  coherence vs number of rephasing pulses  $N$  for samples 12 and 13. Green and orange points are measured with sample 13 at elevated temperatures.

comparable to spin-orbit coupling ( $\sim 48$  GHz), the orbital components of the qubit states are no longer orthogonal [24], leading to an allowed magnetic dipole transition [21]. This MW transition is allowed for both aligned and misaligned magnetic fields, allowing simultaneous MW control and single-shot readout of the  $\text{SiV}^-$  spin.

We focus on single  $\text{SiV}^-$  centers placed less than  $2 \mu\text{m}$  from the coplanar waveguide to efficiently drive the qubit transition with low MW powers and maintain a steady-state sample temperature below 100 mK. The spin qubit frequency  $f_{\downarrow\uparrow}$  is determined using a pulsed optically detected magnetic resonance (ODMR) measurement, as shown in Figs. 3(a) and 3(b). A long laser pulse at frequency  $f_{\downarrow\downarrow}$  initializes the spin in state  $|\uparrow\rangle$  via optical pumping. After a MW pulse of duration  $\tau$ , a second laser pulse at  $f_{\downarrow\downarrow}$  reads out the population in state  $|\downarrow\rangle$ . Once the ODMR resonance is found by scanning the MW frequency [Fig. 3(b)], we drive the qubit transition on resonance and observe Rabi oscillations [Fig. 3(c)]. Finally, we use Ramsey interference to measure the spin dephasing time  $T_2^*$  for both samples [Fig. 3(d)]. For sample 12, which contains a low density of nuclear spins (blue circles), we measure a dephasing time in the range of  $T_2^* = 1.5$  to  $13 \mu\text{s}$ . For this sample, we find that  $T_2^*$  scales inversely with the qubit frequency  $f_{\uparrow\downarrow}$ , as shown in Fig. 3(e). The observed scaling  $T_2^* \propto 1/f_{\uparrow\downarrow}$  indicates that fluctuations of the electronic  $g$  factor  $\Delta g$  likely limit the  $T_2^*$  via the relation  $1/(T_2^*) \propto \Delta g \mu_B B$ , where  $\mu_B$  is the Bohr magneton. Possible origins for  $\Delta g$  are discussed in the Supplemental Material [25]. For sample 13, which contains a natural abundance of nuclear spins (red squares), we measure  $T_2^* \approx 300$  ns independent from the magnetic field magnitude, which is similar to typical values observed with  $\text{NV}^-$  centers. These results demonstrate that the dephasing time  $T_2^*$  of  $\text{SiV}^-$  centers in sample 13 is primarily limited by the nuclear spin bath in the diamond host with a natural abundance of  $^{13}\text{C}$  [30].

Dephasing due to slowly evolving fluctuations in the environment (e.g., nuclear spins) can be suppressed by using dynamical decoupling techniques [31,32]. We extend the spin coherence time  $T_2$  by implementing Carr-Purcell-Meiboom-Gill (CPMG) sequences with  $N = 1, 2, 4, 8, 16,$  and  $32$  rephasing pulses [33] in sample 12 [Fig. 4(b)]. Figure 4(c) shows that the coherence time increases approximately linearly with the number of rephasing pulses  $N$ . The longest observed coherence time is  $T_2 = 13 \pm 1.7$  ms for  $N = 32$ . We also implement CPMG sequences for  $N = 1, 2,$  and  $4$  in sample 13 and find similar coherence times  $T_2$  as for sample 12 [Fig. 4(c)]. We repeat the CPMG measurements at higher temperatures: at 400 mK, the  $T_2$  time measured by CPMG2 is identical to  $T_2$  at 100 mK (red and orange data). At a temperature of 600 mK, the spin echo (CPMG1)  $T_2$  is dramatically reduced to  $60 \mu\text{s}$ . Spin echo measurements with sample 13 at a weak magnetic field of 0.2 kG show high-visibility

oscillations of the electronic spin coherence [25]. These dynamics are suppressed at stronger fields [25] and are characteristic of coherent coupling to nearby  $^{13}\text{C}$  nuclear spins [30].

Surprisingly, the observation in Fig. 4 that the coherence time  $T_2$  in both samples is identical for a given  $N$  indicates that the coherence time  $T_2$  is not limited by the nuclear spin bath, but by another noise source. This observation is also supported by the approximately linear scaling ( $T_2 \sim N$ ) of coherence with the number of  $\pi$  pulses, which deviates substantially from the expected  $\sim N^{2/3}$  scaling for dipolar coupling to nuclear spins [34,35]. We also do not find a significant difference between  $T_2$  measured at different magnetic fields [25], suggesting that  $g$ -factor fluctuations are also not the limiting factor for these measurements.

While the origin of the noise source is at present not understood, the linear dependence of  $T_2$  on  $N$  suggests that  $T_2$  can potentially be further improved by using additional rephasing pulses. In the current measurements, errors due to imperfect  $\pi$  pulses [25] result in reduced state fidelities for pulse sequences with  $N \geq 32$ . Pulse errors can be reduced by using decoupling sequences with two-axis (XY) control [32]. The gate fidelities can also be improved using higher MW Rabi frequencies [25] that can be obtained with low-loss superconducting coplanar waveguides [36].

These observations establish the  $\text{SiV}^-$  center as a promising solid-state quantum emitter for the realization of quantum network nodes using integrated diamond nanophotonics [16]. Although understanding the noise bath and its effects on the  $\text{SiV}^-$  spin dynamics is an important area of future study, the demonstrated coherence time of 13 ms is already sufficient to maintain quantum states between quantum repeater nodes separated by  $10^3$  km [2]. The quantum memory lifetime could be further extended by implementing robust dynamical decoupling schemes [32] or using coherently coupled nuclear spins as longer-lived memories [37]. The  $\text{SiV}^-$  spin could also be strongly coupled to localized acoustic [38,39] modes by exploiting the large strain susceptibility of the  $\text{SiV}^-$  centers (PHz per unit strain) [38]. This offers new opportunities for realizing two-qubit gates [40–42] and interfacing superconducting quantum circuits with long-lived spin memories and optical photons [43].

We thank J. Doyle and D. Patterson for providing cryogenic equipment and expertise; M. Markham, A. Edmonds, and D. Twitchen from Element Six Inc. for providing the samples used in this work; A. Faraon, J. Kindem, and T. Zhong for assistance in the early stages of the experiment; and M. Lončar and H. Park for useful discussions. This work was supported by DURIP Grant No. N00014-15-1-28461234 through ARO, NSF, CUA, AFOSR MURI, and ARL. Coplanar waveguides were fabricated at the Harvard CNS supported under NSF Grant No. ECS-0335765.

D. D. S., A. S., and C. T. N. contributed equally to this work.

*Note added.*—Recently, we became aware of a complementary experiment by Becker *et al.* [44], demonstrating all-optical coherent manipulation of the SiV<sup>-</sup> spin qubit at ~20 mK with an observed coherence time of ~140 ns limited by other impurities in the sample.

\*sukachev@fas.harvard.edu

†lukin@physics.harvard.edu

- [1] H.-J. Briegel, W. Dür, J. I. Cirac, and P. Zoller, *Phys. Rev. Lett.* **81**, 5932 (1998).
- [2] L. Childress, J. M. Taylor, A. S. Sørensen, and M. D. Lukin, *Phys. Rev. Lett.* **96**, 070504 (2006).
- [3] S. Ritter, C. Nölleke, C. Hahn, A. Reiserer, A. Neuzner, M. Uphoff, M. Mücke, E. Figueroa, J. Bochmann, and G. Rempe, *Nature (London)* **484**, 195 (2012).
- [4] D. Hucul, I. Inlek, G. Vittorini, C. Crocker, S. Debnath, S. Clark, and C. Monroe, *Nat. Phys.* **11**, 37 (2015).
- [5] W. B. Gao, A. Imamoglu, H. Bernien, and R. Hanson, *Nat. Photonics* **9**, 363 (2015).
- [6] P. Lodahl, S. Mahmoodian, and S. Stobbe, *Rev. Mod. Phys.* **87**, 347 (2015).
- [7] D. Press, K. De Greve, P. L. McMahon, T. D. Ladd, B. Friess, C. Schneider, M. Kamp, S. Höfling, A. Forchel, and Y. Yamamoto, *Nat. Photonics* **4**, 367 (2010).
- [8] G. Balasubramanian, P. Neumann, D. Twitchen, M. Markham, R. Kolesov, N. Mizuochi, J. Isoya, J. Achard, J. Beck, J. Tissler, V. Jacques, P. R. Hemmer, F. Jelezko, and J. Wrachtrup, *Nat. Mater.* **8**, 383 (2009).
- [9] A. Faraon, C. Santori, Z. Huang, V. M. Acosta, and R. G. Beausoleil, *Phys. Rev. Lett.* **109**, 033604 (2012).
- [10] B. Hensen, H. Bernien, A. E. Dreau, A. Reiserer, N. Kalb, M. S. Blok, J. Ruitenber, R. F. L. Vermeulen, R. N. Schouten, C. Abellan, W. Amaya, V. Pruneri, M. W. Mitchell, M. Markham, D. J. Twitchen, D. Elkouss, S. Wehner, T. H. Taminiau, and R. Hanson, *Nature (London)* **526**, 682 (2015).
- [11] A. Delteil, Z. Sun, W. B. Gao, E. Togan, S. Faelt, and A. Imamoglu, *Nat. Phys.* **12**, 218 (2016).
- [12] E. Neu, D. Steinmetz, J. Riedrich-Möller, S. Gsell, M. Fischer, M. Schreck, and C. Becher, *New J. Phys.* **13**, 025012 (2011).
- [13] L. J. Rogers, K. D. Jahnke, T. Teraji, L. Marseglia, C. Müller, B. Naydenov, H. Schauffert, C. Kranz, J. Isoya, L. P. McGuinness, and F. Jelezko, *Nat. Commun.* **5**, 4739 (2014).
- [14] A. Sipahigil, K. D. Jahnke, L. J. Rogers, T. Teraji, J. Isoya, A. S. Zibrov, F. Jelezko, and M. D. Lukin, *Phys. Rev. Lett.* **113**, 113602 (2014).
- [15] R. E. Evans, A. Sipahigil, D. D. Sukachev, A. S. Zibrov, and M. D. Lukin, *Phys. Rev. Applied* **5**, 044010 (2016).
- [16] A. Sipahigil, R. E. Evans, D. D. Sukachev, M. J. Burek, J. Borregaard, M. K. Bhaskar, C. T. Nguyen, J. L. Pacheco, H. A. Atikian, C. Meuwly, R. M. Camacho, F. Jelezko, E. Bielejec, H. Park, M. Lončar, and M. D. Lukin, *Science* **354**, 847 (2016).
- [17] L. J. Rogers, K. D. Jahnke, M. H. Metsch, A. Sipahigil, J. M. Binder, T. Teraji, H. Sumiya, J. Isoya, M. D. Lukin, P. Hemmer, and F. Jelezko, *Phys. Rev. Lett.* **113**, 263602 (2014).
- [18] B. Pingault, J. N. Becker, C. H. H. Schulte, C. Arend, C. Hepp, T. Godde, A. I. Tartakovskii, M. Markham, C. Becher, and M. Atatüre, *Phys. Rev. Lett.* **113**, 263601 (2014).
- [19] K. D. Jahnke, A. Sipahigil, J. M. Binder, M. W. Doherty, M. Metsch, L. J. Rogers, N. B. Manson, M. D. Lukin, and F. Jelezko, *New J. Phys.* **17**, 043011 (2015).
- [20] J. N. Becker, J. Görlitz, C. Arend, M. Markham, and C. Becher, *Nat. Commun.* **7**, 13512 (2016).
- [21] B. Pingault, D.-D. Jarausch, C. Hepp, L. Klintberg, J. N. Becker, M. Markham, C. Becher, and M. Atatüre, *Nat. Commun.* **8**, 15579 (2017).
- [22] The neutral SiV center (SiV<sup>0</sup>) features suppressed phonon-induced dephasing of its spin state [see Ref. [23] and Green, *Phys. Rev. Lett.* **119**, 096402 (2017)], yielding coherence times of  $T_2 \sim 200$  ms in bulk measurements at  $T = 15$  K (Rose, arXiv:1706.01555). However, their optical properties, including radiative quantum efficiency, are currently believed to be inferior to those of SiV<sup>-</sup> [U. F. S. D’Haenens-Johansson, *Phys. Rev. B* **84**, 245208 (2011)], making it challenging to realize an efficient photonic interface.
- [23] A. M. Edmonds, M. E. Newton, P. M. Martineau, D. J. Twitchen, and S. D. Williams, *Phys. Rev. B* **77**, 245205 (2008).
- [24] C. Hepp, T. Müller, V. Waselowski, J. N. Becker, B. Pingault, H. Sternschulte, D. Steinmüller-Nethl, A. Gali, J. R. Maze, M. Atatüre, and C. Becher, *Phys. Rev. Lett.* **112**, 036405 (2014).
- [25] See Supplemental Material <http://link.aps.org/supplemental/10.1103/PhysRevLett.119.223602> for details on experimental setup, optical pumping, spin manipulation, and noise bath models, which includes additional Refs. [26,27].
- [26] N. Bar-Gill, L. Pham, C. Belthangady, D. Le Sage, P. Cappellaro, J. Maze, M. Lukin, A. Yacoby, and R. Walsworth, *Nat. Commun.* **3**, 858 (2012).
- [27] M. J. Biercuk and H. Bluhm, *Phys. Rev. B* **83**, 235316 (2011).
- [28] L. Robledo, L. Childress, H. Bernien, B. Hensen, P. F. A. Alkemade, and R. Hanson, *Nature (London)* **477**, 574 (2011).
- [29] A. Delteil, W. B. Gao, P. Fallahi, J. Miguel-Sanchez, and A. Imamolu, *Phys. Rev. Lett.* **112**, 116802 (2014).
- [30] L. Childress, M. V. Gurudev Dutt, J. M. Taylor, A. S. Zibrov, F. Jelezko, J. Wrachtrup, P. R. Hemmer, and M. D. Lukin, *Science* **314**, 281 (2006).
- [31] C. A. Ryan, J. S. Hodges, and D. G. Cory, *Phys. Rev. Lett.* **105**, 200402 (2010).
- [32] G. de Lange, Z. H. Wang, D. Ristè, V. V. Dobrovitski, and R. Hanson, *Science* **330**, 60 (2010).
- [33] S. Meiboom and D. Gill, *Rev. Sci. Instrum.* **29**, 688 (1958).
- [34] N. Bar-Gill, L. Pham, A. Jarmola, D. Budker, and R. Walsworth, *Nat. Commun.* **4**, 1743 (2013).
- [35] J. Medford, Ł. Cywiński, C. Barthel, C. M. Marcus, M. P. Hanson, and A. C. Gossard, *Phys. Rev. Lett.* **108**, 086802 (2012).

- [36] A. J. Sigillito, H. Malissa, A. M. Tyryshkin, H. Riemann, N. V. Abrosimov, P. Becker, H.-J. Pohl, M. L. Thewalt, K. M. Itoh, J. J. Morton *et al.*, *Appl. Phys. Lett.* **104**, 222407 (2014).
- [37] P. C. Maurer, G. Kucsko, C. Latta, L. Jiang, N. Y. Yao, S. D. Bennett, F. Pastawski, D. Hunger, N. Chisholm, M. Markham, D. J. Twitchen, J. I. Cirac, and M. D. Lukin, *Science* **336**, 1283 (2012).
- [38] Y.-I. Sohn, S. Meesala, B. Pingault, H. A. Atikian, J. Holzgrafe, M. Gundogan, C. Stavrakas, M. J. Stanley, A. Sipahigil, J. Choi *et al.*, [arXiv:1706.03881](https://arxiv.org/abs/1706.03881).
- [39] M. J. Burek, J. D. Cohen, S. M. Meenehan, N. El-Sawah, C. Chia, T. Ruelle, S. Meesala, J. Rochman, H. A. Atikian, M. Markham, D. J. Twitchen, M. D. Lukin, O. Painter, and M. Lončar, *Optica* **3**, 1404 (2016).
- [40] J. Majer, J. M. Chow, J. M. Gambetta, J. Koch, B. R. Johnson, J. A. Schreier, L. Frunzio, D. I. Schuster, A. A. Houck, A. Wallraff, A. Blais, M. H. Devoret, S. M. Girvin, and R. J. Schoelkopf, *Nature (London)* **449**, 443 (2007).
- [41] S. D. Bennett, N. Y. Yao, J. Otterbach, P. Zoller, P. Rabl, and M. D. Lukin, *Phys. Rev. Lett.* **110**, 156402 (2013).
- [42] K. Stannigel, P. Rabl, A. S. Sørensen, M. D. Lukin, and P. Zoller, *Phys. Rev. A* **84**, 042341 (2011).
- [43] M. V. Gustafsson, T. Aref, A. F. Kockum, M. K. Ekström, G. Johansson, and P. Delsing, *Science* **346**, 207 (2014).
- [44] J. N. Becker, B. Pingault, D. Groß, M. Gündoan, N. Kukharchyk, M. Markham, A. Edmonds, M. Atatüre, P. Bushev, and C. Becher, [arXiv:1708.08263](https://arxiv.org/abs/1708.08263).